PHYSICAL ANALYSIS OF LIGHT-SCATTERING CHANGES IN BOVINE PHOTORECEPTOR MEMBRANE SUSPENSIONS

M. MICHEL-VILLAZ, ALAIN BRISSON, AND YVES CHAPRON
Laboratoire de Biologie Moléculaire et Cellulaire, Département de Recherche Fondamentale, Centre d'Etudes Nucléaires de Grenoble, 85 X, 38041 Grenoble, France

HELEN SAIBIL
Biophysics Department, University of London King's College, London WC2, England

ABSTRACT We have used electron microscopy and model calculations to analyze the physical basis of light-scattering signals from suspensions of photoreceptor membranes. These signals have previously been used to probe interactions between photoactivated rhodopsin (R*) and the peripheral membrane enzyme, GTP-binding protein (G) (Kühn et al., 1981, *Proc. Natl. Acad. Sci. USA.*, 78:6873–6877). Although there is no unique physical interpretation of these signals, we have shown in this study that they were qualitatively unchanged when the rod outer segment fragments (containing stacked disks) were fragmented by sonication or osmotic shock to produce spherical disk membrane vesicles. An exact treatment of the scattering process for spherical vesicles enabled us to evaluate the effects of changing membrane thickness, refractive index, or vesicle diameter. We present a particular redistribution of mass upon R*-G interaction that fits the experimental data.

INTRODUCTION

The turbidity of biological suspensions originates from light-scattering of particles such as cells, subcellular fragments, or vesicles similar in magnitude to the wavelengths in the visible spectrum. This turbidity is generated by attenuation and distortion (in wavelength, direction, and sometimes polarization) of the incident light beam. Changes in light-scattering signals induced by rhodopsin photoexcitation in rod outer segment (ROS) suspensions have been observed in several laboratories (1–8). When interpreted, they have been assumed to correspond to changes in size or separation of the disks: rod swelling (4) or shrinkage (2, 9) as a consequence of primary events following the bleaching of rhodopsin. As far as we know, the first study showing a relationship between such changes in turbidity and the functioning of the enzymes involved in cGMP phosphodiesterase activation is by Bignetti et al. (10). Subsequently, we described three different kinds of photo-induced light-scattering signals (7) (see Fig. 1): (*a*) a rhodopsin signal associated with the meta I → meta II transition (11); (*b*) a binding signal, related to R*-G complex formation, and (*c*) a so-called dissociation signal observed when GTP is present, related to nucleotide exchange and dissociation of the complex and synchronous with the triggering of phosphodiesterase activity (12). The binding and dissociation signals were shown to depend specifically on the presence of G. To physically analyze these signals, we characterize the preparations from which they can be obtained and refer to the physical theories of light scattering. A simple model, in which the membranes are represented as shells of variable diameter, thickness, and refractive index, leads to reasonable although not unique conclusions.

METHODS

Preparations of rod membranes, washed disks, and soluble protein extracts are obtained as previously indicated (7). The standard buffer used for all light-scattering experiments is 100 mM KCl, 1 mM $MgCl_2$, 10 mM Tris HCl (pH 7.4), 1 mM dithiothreitol. ROS are purified from fresh bovine retinae and are stored frozen as pellets at −80°C. Pellets are homogenized with buffer followed by passage through a syringe needle. This treatment yields suspensions of fragmented rod membranes. These membranes are then homogenized in 5 mM Tris HCl (pH 7.4) and centrifuged (20 min at 80,000*g*). The clear supernatant is the soluble protein extract. The pellet is resuspended and recentrifuged in 5 mM Tris HCl to provide the washed disk preparation, which is homogenized and resuspended in standard buffer. All relevant details that do not appear in this paper (cuvette position, light excitation, etc.) are dealt with in the above-mentioned paper. Here we cover only the technique used to record signals.

Light-Scattering Signal

A Durrum D-117 spectrometer (Durrum Instrument Corporation, Palo Alto, CA) was used to record light-scattering variations. The variations appear either as transmittance changes in the measuring beam (forward scattering, scattering angle 0°) or as variations in the beam scattered at 90° to the measuring beam. The measuring beam comes from a monochromator that supplies a set wavelength to an ~1-nm bandwidth. The photomultiplier is equipped with an interference filter of the same

Helen Saibil's present address is the Department of Zoology, University of Oxford, South Parks Road, Oxford, England.

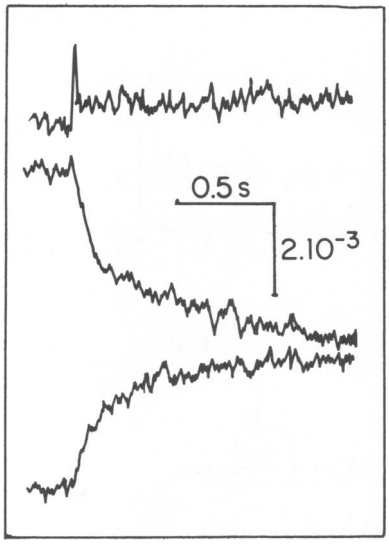

FIGURE 1 Light-induced scattering signals at 20°C and pH 7.5. The *upper* trace shows rhodopsin signal from washed disks induced by a flash bleaching 8%. The *middle* trace shows in absence of GTP, the binding signal from ROS fragments, induced by 4% bleaching. The signal amplitude is not saturated. The *lower* trace shows the dissociation signal in presence of $|GTP| = 42\ \mu M$ induced by a flash bleaching 4%. The amplitude of the dissociation signal from ROS fragments is saturated by 0.5% bleaching. Rhodopsin concentration = 3 μM. The vertical scale is the relative transmitted intensity change.

wavelength to protect it from any other wavelength and above all that of the bleaching flash. Most measurements were made using forward scattering (see Fig. 2). The photomultiplier receives beams scattered in a cone with a half aperture ~7°, with the photomultiplier in its usual position (inlet 6 cm away from the cuvette). Thus, our spectrometer lacks accuracy as far as angular resolution is concerned and is certainly not the most suitable for detailed studies of light scattering. However, it is simple and adequate for the present analysis. The transmitted light intensities are recorded as follows. The transmittance of the cuvette filled with suspension buffer is measured. The wavelength, usually 700 nm, is selected outside the absorption bands of the membranes, which are added subsequently. The input voltage of the photomultiplier is set so that the output amplifier of the photomultiplier produces a signal of 10 V. The addition of membranes to the cuvette lowers the output signal from the photomultiplier to the level I_R (which is typically ~5 V), in proportion to the quantity of light scattered over all space outside the entrance gate of the photomultiplier. The variations ΔI_R that occur about this level are monitored accurately by an amplifier with an offset system. ΔI_R is expressed either as electric units (voltage variations at photomultiplier output, e.g., 50 mV), or as relative variation, $\Delta I_R/I_R$, e.g., 50 mV compared with 5 V, i.e., $\Delta I_R/I_R = 10^{-2}$, or as optical density variation $\Delta OD = 0.43 \times 10^{-2}$ since $OD = \log_{10}(I_0/I_R)$.

Electron Microscopy

Negative Staining. Samples (0.1–0.5 mg rhodopsin/ml) were deposited on formvar-carbon coated grids rendered hydrophilic by air glow discharge and were negatively stained with 1% phosphotungstic acid at pH 7.0.

Thin Sectioning. Samples were fixed in 0.1 M Na cacodylate (pH 7.2) containing 2.5% glutaraldehyde and 1% tannic acid for 1½ h at 4°C. After centrifugation for 10 min at 12,000 rpm, pellets were postfixed in 1% OsO_4 in 0.1 M Na cacodylate pH 7.2 for 2 h at 4°C. Samples were dehydrated in an ethanol-acetone series and embedded in Epon 812, an epoxyresin (Balzers, Liechtenstein). Thin sections were stained with 1% uranyl acetate in 50% ethanol for 10 min followed by lead citrate for 5 min. Observations were made on a JEOL 100S electron microscope at 80 kV (JEOL Ltd., Akishima, Tokyo, Japan).

Calculations

Calculations were done using an Apple II 56 K computer (Apple Computer Inc., Cupertino, CA) operating with microsoft CPM and Basic Language. The scattered intensity is calculated as the sum of a series, each term of which depends on special mathematical functions (Bessel-Riccati and modified Legendre). We have developed the subroutines for these mathematical functions.

RESULTS

Calibration of Light-induced Scattering Changes

Fig. 1 shows binding and dissociation signals from suspensions of ROS fragments as described in reference 7. The origin of I_R and ΔI_R is shown schematically in Fig. 2. In a given preparation, the signals studied with a set analyzing wavelength increase with the quantity of membranes added to the cuvette. The initial scattering level, $I_0 - I_R$ also varies with amount of membranes in the cuvette. This level can be expressed by the optical density, $OD = \log_{10}(I_0/I_R) = \log_{10}\{10/[10 - (I_0 - I_R)]\}$, where $I_0 - I_R$ is expressed in volts. Fig. 3 shows how the relationship between the relative transmitted light change expressed in units of ΔOD and the initial scattering level (binding [○] and dissociation [▲]) is affected by the ROS membrane concentration. The relationship is linear in the limit where membranes are dilute and in this case the limiting value of $\Delta OD/OD$ averages 1% for binding signals. The curve in Fig. 3 provides the experimental calibration for measuring light-scattering changes.

Changes in pH and temperature modify the light-induced signals, implying that metarhodopsin II triggers these signals (11). But at constant pH and temperature, changes in scattering parameters such as analyzing wavelength or average size of scattering objects affect I_R and ΔI_R. But it is remarkable that their relationship (plotted in Fig. 3) falls on the same curve. In particular, we altered the size of the scattering fragments using a sonication process of variable duration, until we obtained small disk vesicles as shown in Fig. 4. With aliquots from the same original suspension, we obtained the points (·) shown in Fig. 3, fitting on the same curve. We also modified the analyzing wavelength in the range of 600 to 850 nm, so as to remain outside the absorption band of the rhodopsin and this gave points (▽) located on the same curve. This result shows that whatever the parameter ranges selected, the light-induced intensity change is related to initial light-scattering intensity level in darkness. The fact that samples as diverse as ROS fragments and disk vesicles show light-induced responses fitting the same calibration curve suggests that

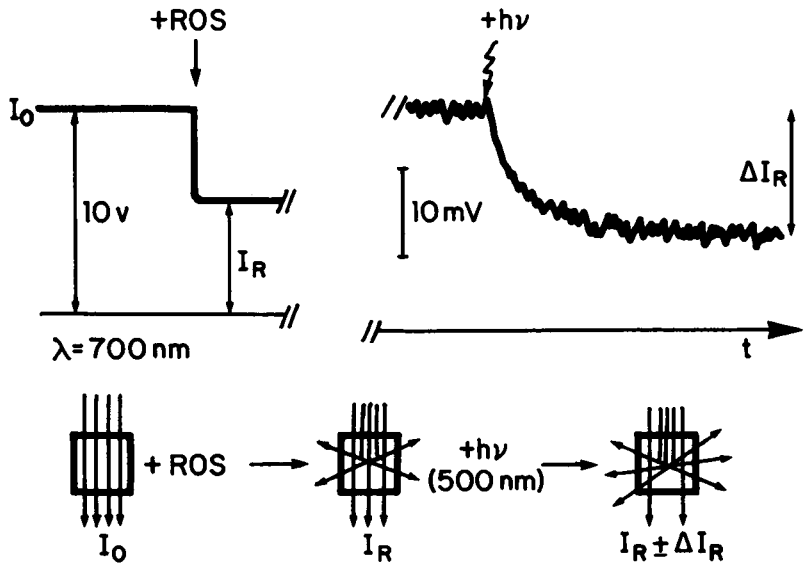

FIGURE 2 Schematic diagram of the scattering measurements. (*Top*) Before the membranes are added, the total intensity of the measuring beam, I_0, is recorded on the photomultiplier. After membrane addition, the analyzing beam is scattered and only I_R reaches the photomultiplier entrance gate. Photoexcitation of the rhodopsin at 500 nm induced small changes of the scattering level. Note the amplification of scales between the left and right sides. (*Bottom*) View of the cuvette from above. The measuring beam (700 nm) is shown symbolically, in the same conditions as in the upper part of the figure. First, the unscattered beam is shown, then scattering due to the addition of unbleached membranes and finally the scattering change induced by the bleaching flash. Increased scattering corresponds to decreased forward transmittance.

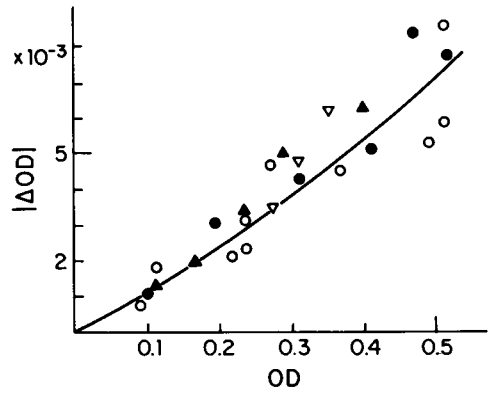

FIGURE 3 Calibration of the light-scattering changes. *OD* represents the initial level of scattered light outside the entrance gate of the photomultiplier, $|\Delta OD|$ is the absolute value of the amplitude at saturation of either the binding or the dissociation signal (note that these signals have opposite signs). $I_0 - I_R$ and ΔI_R are measured by the output voltage of the photomultiplier and *OD* and ΔOD are calculated from these values by the formula in the text. The amplitude of the binding signal includes the slow components of the signal when they are present. In the case of the reconstituted system where there is a slow decay of the dissociation signal, ΔI_R is taken as the amplitude of the rising phase of the signal. ○ indicates the binding signals with different amounts of ROS fragments ranging from 1.3 to 6.5 μM rhodopsin concentration. ● indicates the binding signals for ROS fragments at 6.5 μM rhodopsin sonicated with variable strength. ▲ indicates the dissociation signals with different amounts of ROS fragments, from 1.3 to 5.2 μM rhodopsin concentration and 20 μM GTP. We do not compare the amplitudes of binding and dissociation signals for a given sample because the dissociation signal is more sensitive to the state of the sample and can decrease independently. ▽ indicates the binding signals observed at three different wavelengths (600, 700, and 800 nm). All signals are recorded at 20°C, pH 7.4.

the simplest model (membranes seen as spherical shells) provides a realistic picture of the scattering process.

Influence of Parasitic Scattering

We tested the influence of a parasitic scattering substance in the sample. We added latex balls (diameter 1–2 μm) to the rod fragment suspension, thus increasing the initial scattering level, $I_0 - I_R$, with these extraneous static scatterers. We measured the binding signals as before. The light-induced signals, $\Delta I_R/I_R$, were independent of the number of latex balls added. This indicates that parasitic scattering does not cause any light-induced change and does not interfere with photo-induced signal recording. The proportionality between $\Delta I_R/I_R$ and the membrane scattering is thus unmodified. It confirms that the phenomenon observed originates from the photoreceptor membrane themselves. On other biological samples that could be contaminated by scattering impurities (actin filaments, cytoskeleton, ...) it excludes any perturbation by parasitic scatterers. It is particularly useful for the study of cephalopod photoreceptors (Saibil, H., and M. Michel-Villaz, manuscript submitted for publication).

Wavelength Dependence

We recorded an absorption spectrum of the rod fragment preparation and found a scattering background with a $1/\lambda^2$ wavelength dependence. This is expected when the size of the analyzed objects is greater than the analyzing wavelength, as shown by our electron microscopy. The scatter-

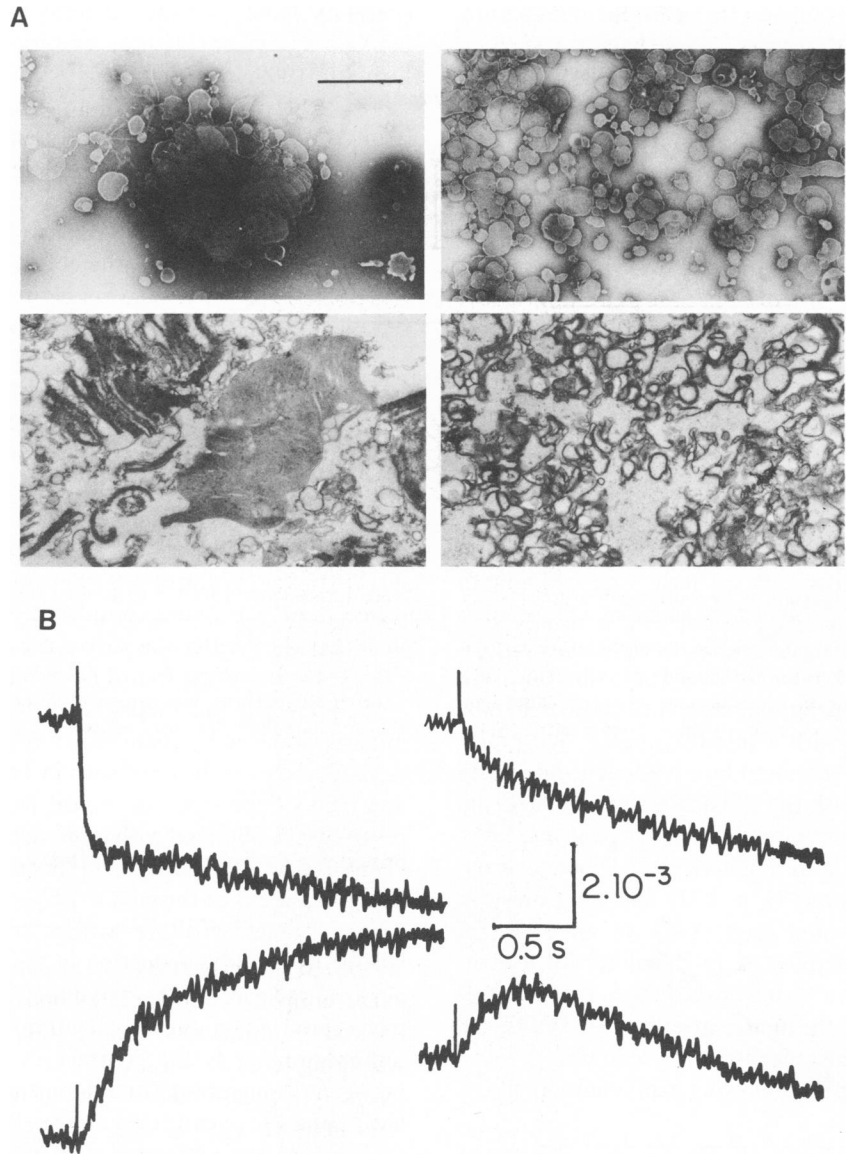

FIGURE 4 Membrane geometry and light-scattering signals for ROS fragments and rhodopsin vesicles. (*A*) Electron micrographs of our two types of preparation: ROS fragments (*left*) and rhodopsin vesicles (*right*) observed after negative staining (*top*) or thin sectioning (*bottom*). The rhodopsin vesicles are obtained either by transient hypotonic shock and are then depleted of peripheral proteins that are added for the measurements, or by sonication. The bar represents 2 μm. (*B*) Light-scattering signals of the two types of preparations, binding signals (*top*) and dissociation signals (*bottom*) in presence of 18 μM GTP, obtained on ROS fragments (*left*) (rhodopsin concentration 4.2 μM) and rhodopsin vesicles with added soluble protein extract (*right*) (rhodopsin concentration 4.6 μM and GTP binding protein concentration estimated to be 0.36 μM, i.e., about the ¾ of the native concentration). The initial scattering level for the rhodopsin vesicles is 60% of the initial scattering level for the ROS fragments. Temperature 20°C, pH 7.4.

ing background for disk vesicles is, as expected, considerably lower (with the same rhodopsin concentration $I_0 - I_R$ is reduced by ~2) but has a spectral dependence close to $1/\lambda^4$, which is expected for Rayleigh scattering from small particles.

Electron Microscopy

Both types of preparation (ROS fragments and rhodopsin vesicles) are represented in Fig. 4 *A* by negative staining and thin sectioning. The ROS fragment suspension mainly consists of stacks of disks, which are often deprived of the rod external membrane. The stacks do not look like a section of a cylinder (the rod) but resemble a toppled stack of books. Some of the books are still stacked, only the edges of others are visible and some of them are dispersed. The resulting objects form 3 to 5 μm ovoid packets. The suspension also contains a minority of disks or fragments of disks. By both negative staining and thin sectioning, the vesicle suspension proved quite homogeneous. No object is greater than the disk diameter. The average diameter from the photographs obtained with negative staining is 0.6 μm.

The thin-section pictures suggest that most membranes are approximately spherical vesicles. These pictures show a very small number of disk-shaped objects that were not revealed by negative staining.

For both kinds of membranes (ROS fragments containing stacked disks, and roughly spherical rhodopsin vesicles with added soluble protein extract) binding and dissociation signals were observed (Fig. 4 *B*). They are qualitatively identical (binding saturation with the stoichiometry of the GTP binding protein, dissociation saturation at low bleaching level). The differences often observed in the case of rhodopsin vesicles with recombined enzyme extract consist of slowing down of the signal kinetics and a slow decay of the dissociation signal.

Calculations of Static Scattering

A comprehensive treatment of theories and approaches used for the description of light scattering can be found in Kerker (1969) (13). For suspensions of biological particles whose size is of the same range as the wavelength, the most popular theory is the Rayleigh-Gans approximation. We did not make use of this approximation but chose to handle the exact calculations with a microcomputer. We evaluated the light intensity scattered by a homogeneous sphere (to check agreement with the classical results by Mie and Van de Hulst), and then to mimic the biological vesicle we calculated the scattering by a spherical shell (two concentric spheres, see Kerker [13], p. 193) and by a dielectic bubble (i.e., a thin-walled shell [14]). In all cases the programs developed enabled us to calculate, for a given wavelength, the total scattering cross section, C_s, as well as the angular intensity of the light-scattering $I_s(\theta)$ multiplied by $4\pi r^2$ where r is the distance from the scatterer.

For all three models, the following expressions apply

$$C_s = \frac{\lambda^2}{2\pi} \sum_{n=1}^{\infty} (2n+1)\,(|a_n|^2 + |b_n|^2); \qquad (1)$$

$$I_s(\theta) = \frac{\lambda^2}{2\pi} \left\{ \left| \sum_{n=1}^{\infty} \frac{2n+1}{n(n+1)} \cdot [a_n \pi_n(\cos\theta) + b_n \tau_n(\cos\theta)] \right|^2 + \left| \sum_{n=1}^{\infty} \frac{2n+1}{n(n+1)} \cdot [a_n \tau_n(\cos\theta) + b_n \pi_n(\cos\theta)] \right|^2 \right\}, \qquad (2)$$

in which π_n and τ_n are modified Legendre functions and are solutions of the scattering problem in spherical geometry with axial anisotropy, and in which a_n and b_n are the complex scattering coefficients depending on the shape of the scattering object. The coefficients are given in the Appendix. They depend on Bessel-Riccati functions ψ_n and ζ_n for spherical shapes. The numerical convergence of the series providing C_s and $I_s(\theta)$ is obtained with a few terms (between 3 and 7 for the generally used values of parameters), in agreement with an empirical rule discovered by Debye in 1909.

We obtained identical numerical results both for a bubble and a shell when the difference between the inside diameter and the outside diameter equals the bubble thickness. It is therefore possible to calculate the intensities scattered by a spherical vesicle for a given analyzing wavelength and three parameters: diameter ϕ, thickness d, and relative refractive index m between the membrane and its environment (internal and external medium are assumed to be identical). The results of this calculation are qualitatively identical with those obtained for light-scattering on a solid sphere, namely, that scattering is an oscillatory function (cf., reference 15, p. 662). For a given set of parameters (size, wavelength), the same variation (in size, for example) may either increase or decrease scattering, depending on whether total scattering C_s, forward scattering $I_s(0)$, or scattering at right angles to the analyzing beam $I_s(\pi/2)$ is being considered. The calculations confirm that the greater the size of the scattering objects, the greater the deviation from $1/\lambda^4$ behavior.

We now use this method to calculate the variations in intensity induced by changes in any of the relevant parameters. Sample results are shown in Table I. It is the case for any model depending on several parameters that a given result can be obtained with more than one set of parameter values. Thus, a 3% decrease in forward scattering $I_s(0)$ can be obtained either through a 1.5% reduction in the membrane thickness d (other parameters remaining unmodified) or by a 0.12% reduction in the relative index m (the geometrical parameters remaining constant). As for neutron scattering on partially deuterated objects, one important parameter is the contrast in the refractive indices between the membrane and the suspension, and the other is the apparent scattering mass represented here by $(m-1)d$. Any observed scattering change reveals an overall change in the latter parameter originating from changes in either m, d, or both. The measured intensity I_R is actually a mixture of total scattering intensity C_s and forward scattering within an angle of 7°. The relative variation of I_R for dilute suspensions is shown in the final column of Table I.

DISCUSSION

Our most striking result has been the identical quality of the signals obtained on preparations of extremely varied geometry, where one might expect different scattering behavior. These preparations include bovine ROS fragments and disk vesicles (Fig. 4) as well as fragments of squid photoreceptor microvilli (Saibil, H., and M. Michel-Villaz, manuscript submitted for publication). The signals from each of these preparations have identical signs, they are dependent in the same way on the protein stoichiometry, and they saturate in the same way with the degree of light excitation. However, differences in kinetics have been

TABLE I
LIGHT SCATTERING BY SPHERICAL VESICLE

	C_s $\times 10^5$	$\frac{\Delta C_s}{C_s}$	$I_s(0)$ $\times 10^4$	$\frac{\Delta I_s}{I_s}$	I_R $\times 10^5$	$\frac{\Delta I_r}{I_r}$
		percent		*percent*		*percent*
A. Reference vesicle $\phi = 0.6\ \mu m$ $d = 60$ Å $m = 1.0806$	5.296	—	5.859	—	5.003	—
B. Vesicle A except refractive index decreased 0.1% (constrast decreased) $\phi = 0.6\ \mu m$ $d = 60$ Å $m = 1.0795$	5.151	−2.74	5.700	−2.71	4.866	−2.74
C. Vesicle A except thickness increased 0.3 Å (mass increased) $\phi = 0.6\ \mu m$ $d = 60.3$ Å $m = 1.0806$	5.348	+0.98	5.917	+0.99	5.052	+0.98
D. Vesicle A except thickness decreased 0.4 Å (mass decreased) $\phi = 0.6\ \mu m$ $d = 59.6$ Å $m = 1.0806$	5.224	−1.36	5.780	−1.35	4.935	−1.36
E. Expanded vesicle ϕ increased and d decreased 0.4 Å such that $\phi^2 d$ remains constant (constant mass) $\phi = 0.602\ \mu m$ $d = 59.6$ Å $m = 1.0806$	5.268	−0.53	5.862	+0.05	4.915	−0.56
F. Expanded vesicle ϕ increased with thickness and refractive index constant (mass increased) $\phi = 0.602\ \mu m$ $d = 60$ Å $m = 1.0808$	5.339	+0.81	5.944	+1.45	5.042	+0.78
G. Vesicle A except d and m changes such that $(m - 1)\ d$ stays constant (constant contrast, volume decreased) $\phi = 0.6\ \mu m$ $d = 59$ Å $m = 1.0820$	5.302	+0.11	5.863	+0.07	5.009	+0.70

The calculations presented are for 700-nm light of unit intensity, incident upon a spherical shell of external diameter ϕ, thickness d, and refractive index m relative to the medium. The reference vesicle is represented in line A: its diameter is estimated from electron microscopy of disk vesicles, its refractive index is taken from values in the literature (21), and the thickness is considered reasonable for a rhodopsin membrane. The precise values chosen for these parameters are unimportant since the variations in scattering are determined by relative changes in the parameters. With respect to the reference vesicle in A, lines B–G show the effect of varying the vesicle parameters. C_s is the total scattering cross section for a single vesicle, $I_s(0)$ is the forward scattering (recorded at distance r and multiplied by $4\pi r^2$). I_r is the measured intensity within an angle of 7° (mixture of total scattering intensity and forward scattering). We checked that the poor angular resolution of our measurements does not affect the results. All the parameter variations envisaged are small compared with the initial values. When this is the case, reversing the direction of the variations simply reverses the sign of the scattering changes, as shown by the comparison of lines C and D. In the discussion, we suggest that line B could represent the rhodopsin signal, and line D the dissociation signal. Regarding the binding signal, a signal with its sign and magnitude can be modeled by either C or F (in both cases, membrane mass increases). Our model does not consider departures from spherical shape.

observed. Whenever the membranes have been modified as a result of sonication or transient osmotic shock, the signals are slowed down. These slight kinetic differences are likely to reflect the outcome of a membrane or enzyme alteration, which hinders the original speed of interaction rather than a new scattering phenomenon.

Our electron micrographs clearly demonstrate the rod fragment and spherical vesicle geometries. Despite the apparent homogeneity of our vesicle suspensions, one can never rule out the possibility that a small number of bigger unwanted objects may play an important part in scattering, as already shown (16). After carefully counting all the vesicles according to their size, we conclude that this is unlikely to be the case in our preparations. For all samples,

the light-induced scattering changes provided points fitting on the same calibration curve (Fig. 3). The similarity of light-scattering signals from the rod fragment and vesicle preparations shows that a spherical vesicle is a valid model for analysis of these signals.

The results of our calculation suggest a straightforward interpretation of the three signals observed. The rhodopsin signal, observed when meta I converts to meta II in the absence of G, corresponds either to membrane thinning or to a decrease in the average refractive index of the membrane. It seems most unlikely that the membrane has become thinner, since the volume of meta II is considered to be greater than the volume of meta I. Studies at high pressure (17, 18) indicate that meta II is more compressible, and thus less compact than meta I. Certain sites of proteolytic attack are made accessible only in meta II (19), suggesting a more unfolded state. Moreover, observations by infrared spectroscopy (20) show that there is no detectable change in α-helix orientation or in the fraction of hydrophobic residues after bleaching of rhodopsin. Thus, it is hard to imagine a meta II volume increase with a reduced membrane thickness. A reduction of the refractive index is therefore a likely explanation of the rhodopsin signal. There is no straightforward evidence in the literature for such a change, though a decrease in intrinsic birefringence ($m_{\parallel} - m_{\perp}$) has been observed related to the appearance of meta II (21, 22).

The binding signal is consistent with an increase in either the average thickness or the refractive index of the membrane or with a combination of the two. Variations in the index of refraction from the bottom to the top of the rod are suggested by changes in birefringence and ascribed to lipid aging (23), but not to interactions with G. Neutron diffraction of rods reveals a light-induced protein mass shift. The protein mass center of gravity is shifted by ~1 Å towards the outside of the disk (24). According to our calculations, such an apparent thickening of the membrane would generate scattering effects of the same magnitude as the ones observed in our binding signal (see Table I). As the G protein is present in the membrane before bleaching, we can only speculate that this apparent thickening is due to a change in the distribution of membrane mass upon interaction of G with rhodopsin.

Because the signals mentioned in former papers (1–4, 9, 16) are obtained without GTP, they should be compared either with our rhodopsin signal or with our binding signal. In fact, the light-induced signals obtained by McConnell (2), by Asai et al. (4), and the signal N obtained by Hofmann et al. (3) are a decrease in light-scattering (increase in the forward transmitted light), and therefore correspond to our rhodopsin signal. The signals P obtained by Hofman et al. (3) appear as an increase in the scattered light, saturate at ~15% bleaching and are thus similar in all respects to our binding signal. Our experimental data are thus in agreement with those already published. But we disagree on interpretation. Uhl et al. (9) propose that the signal P (our binding signal) results from a shrinkage of the disks, based on the fact that the sign of the light-induced signal is the same as the one obtained by hypertonic shock. We feel that the analogous sign is not a strong argument for interpreting the binding signal as a shrinkage. Moreover, light-induced signals may result from changes in the state of membrane aggregation, though controlled by enzymatic processes (8). The fact that the binding signal depends precisely on the presence of G (7) suggests strongly that it is due to intrinsic changes in the membrane caused by protein interactions, independently of osmotic changes.

The dissociation signal corresponds to a decrease in scattering (increase in the forward transmitted light). If it is considered as a change in size, the most straightforward interpretation is that it corresponds to a decrease in the apparent thickness of the membrane of <1 Å for a 60-Å membrane. The GTP binding proteins (1/10 of the rhodopsin in number) form 1/30 to 1/40 of the membrane surface area. A 1-Å apparent change in the average thickness corresponds to eliminating a 30-Å protruding object covering 1/30 of the surface, approximately the room needed for a subunit of the GTP binding protein. Dissociation of the R-G complex as a result of GTP action might release a subunit of the G protein from the membrane in agreement with biochemical evidence (25) though these biochemical findings are not time resolved. This is consistent with the sign of our dissociation signal.

A more detailed physical interpretation of the light-scattering signals would require data on the spatial distribution of refractive index or dielectric constant. The anisotropy of scattering signals has been described for oriented rod suspensions (16, 26) and has permitted a distinction between isotropic changes, changes in the plane of the membrane and normal to the membrane plane. However, to obtain a physical interpretation of these spatially resolved signals, it will be necessary to consider local anisotropy of refractive index.

APPENDIX

The scattering coefficients in the formulas (Eqs. 1 and 2) are given for a spherical shell by (5.1.27) and (5.1.28) in Kerker's book (13)

$$a_n = \frac{\begin{vmatrix} \psi_n'(m\alpha) & \chi_n'(m\alpha) & -m\psi_n'(\alpha) & 0 \\ \psi_n(m\alpha) & \chi_n(m\alpha) & -\psi_n(\alpha) & 0 \\ \psi_n'(m\beta) & \chi_n'(m\beta) & 0 & -m\psi_n'(\beta) \\ \psi_n(m\beta) & \chi_n(m\beta) & 0 & -\psi_n(\beta) \end{vmatrix}}{\begin{vmatrix} \psi_n'(m\alpha) & \chi_n'(m\alpha) & -m\psi_n'(\alpha) & 0 \\ \psi_n(m\alpha) & \chi_n(m\alpha) & -\psi_n(\alpha) & 0 \\ \psi_n'(m\beta) & \chi_n'(m\beta) & 0 & -m\zeta_n'(\beta) \\ \psi_n(m\beta) & \chi_n(m\beta) & 0 & -\zeta_n(\beta) \end{vmatrix}} \quad \text{(A1)}$$

$$b_n = \frac{\begin{vmatrix} \psi_n'(m\alpha) & \chi_n'(m\alpha) & -\psi_n'(\alpha) & 0 \\ \psi_n(m\alpha) & \chi_n(m\alpha) & -m\psi_n(\alpha) & 0 \\ \psi_n'(m\beta) & \chi_n'(m\beta) & 0 & -\psi_n'(\beta) \\ \psi_n(m\beta) & \chi_n(m\beta) & 0 & -m\psi_n(\beta) \end{vmatrix}}{\begin{vmatrix} \psi_n'(m\alpha) & \chi_n'(m\alpha) & -\psi_n'(\alpha) & 0 \\ \psi_n(m\alpha) & \chi_n(m\alpha) & -m\psi_n(\alpha) & 0 \\ \psi_n'(m\beta) & \chi_n'(m\beta) & 0 & -\zeta_n'(\beta) \\ \psi_n(m\beta) & \chi_n(m\beta) & 0 & -m\zeta_n(\beta) \end{vmatrix}} \quad \text{(A2)}$$

where m is the relative refractive index of the shell wall, α and β are $2\pi/\lambda$ times the internal and external radii of the spherical shell, ψ_n, χ_n, and ζ_n are Bessel functions. When the thickness of the shell becomes small compared with the diameter, the boundary conditions for the wave propagation are simplified. Instead of three media and two limit conditions, only one medium with one boundary condition is considered (14). The scattering coefficients are

$$a_n = -i\frac{u|\psi_n'(\alpha)|^2}{I + iu\,\psi_n'(\alpha)\,\zeta_n'(\alpha)}$$

$$b_n = -i\frac{u|\psi_n(\alpha)|^2}{I + iu\,\psi_n(\alpha)\,\zeta_n(\alpha)}$$

where $u = (2\pi/\lambda)\,(d)\,(\Delta\epsilon/\epsilon_0)$. d is the thickness of the membrane, λ is the wavelength, $\Delta\epsilon$ is the variation of dielectric constant between the membrane and its environment of dielectric constant, ϵ_0.

We thank Nelly Bennett for her collaboration in our initial experiments on the light-scattering signals. We also thank Marc Chabre, Hermann Kühn, Yves Dupont, and Guy Paillotin for their interest and discussions. Finally, we thank Michel Ronjat for asssistance with the experiments.

Received for publication 10 October 1983 and in final form 28 May 1984.

REFERENCES

1. Brierley, G. P., D. Fleischman, S. D. Hughes, G. R. Hunter, and D. G. McConnell. 1968. On the permeability of isolated bovine retinal outer segment fragments. *Biochim. Biophys. Acta.* 163:117–120.
2. McConnell, D. G. 1975. Relationship of the light-induced proton uptake in bovine retinal outer segment fragments to triton-induced membrane disruption and to volume changes. *J. Biol. Chem.* 250:1898–1906.
3. Hofmann, K. P., R. Uhl, W. Hoffman, and W. Kreutz. 1976. Measurements of fast light-induced light-scattering and absorption changes in outer segments of vertebrate light sensitive rod cells. *Biophys. Struct. Mech.* 2:61–77.
4. Asai, H., T. Chiba, S. Kimura, and M. Takagi. 1975. A light-induced conformational change in rod photoreceptor disk membrane. *Exp. Eye Res.* 21:259–267.
5. Harary, H. H., J. E. Brown, and L. H. Pinto. 1978. Rapid light-induced changes in near infrared transmission of rods in *bufo marinus*. *Science* (*Wash. DC*). 202:1083–1085.
6. Wey, C. L., and R. A. Cone. 1978. Light-induced light-scattering changes from rod outer segments (ROS). *Biophys. J.* 21(2, Pt. 2):135*a*. (Abstr.)
7. Kühn, H., N. Bennett, M. Michel-Villaz, and M. Chabre. 1981. Interactions between photoexcited rhodopsin and GTP-binding protein: kinetic and stoichiometric analyses from light-scattering changes. *Proc. Natl. Acad. Sci. USA.* 78:6873–6877.
8. Lewis, J. W., J. L. Miller, J. Mendel-Hartvig, L. E. Schaechter, D. S. Kliger, and E. A. Dratz. 1984. Sensitive light-scattering probe of enzymatic processes in retinal rod photoreceptor membranes. *Proc. Natl. Acad. Sci. USA.* 81:743–747.
9. Uhl, R., F. P. Hofmann, and W. Kreutz. 1977. Measurement of fast light induced disk shrinkage within bovine rod outer segments by means of a light-scattering transient. *Biochim. Biophys. Acta.* 469:113–122.
10. Bignetti, E., A. Cavaggioni, P. Fasella, S. Ottonello, and G. L. Rossi. 1980. Light and GTP effects on the turbidity of frog visual membrane suspensions. *Mol. Cell. Biochem.* 30:93–99.
11. Bennett, N., M. Michel-Villaz, and H. Kühn. 1982. Light-induced interaction between rhodopsin and the GTP-binding protein. Metarhodopsin II is the major photoproduct involved. *Eur. J. Biochem.* 127:97–103.
12. Bennett, N. 1982. Light-induced interactions between rhodopsin and the GTP-binding protein relation with phosphodiesterase activation. *Eur. J. Biochem.* 123:133–139.
13. Kerker, M. 1969. The Scattering of Light. Academic Press, Inc., New York. 666 pp.
14. Andreasen, M. G. 1957. Back-scattering cross section of a thin, dielectric, spherical shell. *IRE Trans. Antennas Propagat.* 267–270.
15. Born, M., and E. Wolf. 1975. Principles of Optics. Pergamon Press Inc., Elmsford, NY. Fifth ed. 808 pp.
16. Hofmann, K. P., A. Scheicher, D. Emeis, and J. Reichert. 1981. Light-induced axial and radial shrinkage effects and changes of the refractive index in isolated bovine rod outer segments and disk vesicle. *Biophys. Struct. Mech.* 8:67–93.
17. Lamola, A. A., T. Yamane, and A. Zipp. 1974. Effects of detergents and high pressures upon the metarhodopsin I metarhodopsin II equilibrium. *Biochemistry.* 13:738–745.
18. Attwood, P. V., and H. Gutfreund. 1980. The application of pressure relaxation to the study of the equilibrium between metarhodopsin I and II from bovine retinas. *FEBS* (*Fed. Eur. Biochem. Soc.*) *Lett.* 119:323–326.
19. Kühn, H., O. Mommertz, and P. A. Hargrave. 1982. Light-dependent conformational change at rhodopsin's cytoplasmic surface detected by increased susceptibility to proteolysis. *Biochim. Biophys. Acta.* 679:95–100.
20. Michel-Villaz, M., H. Saibil, and M. Chabre. 1979. Orientation of rhodopsin α-helices in retinal rod outer segment membranes studied by infrared linear dichroism. *Proc. Natl. Acad. Sci. USA.* 76:4405–4408.
21. Liebman, P. A., W. S. Jagger, M. W. Kaplan, and F. G. Bargoot. 1974. Membrane structure changes in rod outer segments associated with rhodopsin bleaching. *Nature* (*Lond.*). 251:31–36.
22. Kaplan, M. W. 1982. Modeling the rod outer segment birefringence change correlated with metarhodopsin II formation. *Biophys. J.* 38:237–241.
23. Kaplan, M. W., M. E. Deffebach, and P. A. Liebmann. 1978. Birefringence measurements of structural inhomogeneities in *Rana pipiens* rod outer segments. *Biophys. J.* 23:59–70.
24. Saibil, H., M. Chabre, and D. Worcester. 1976. Neutron diffraction studies of retinal rod outer segment membranes. *Nature* (*Lond.*). 262:266–270.
25. Emeis, D., N. Kühn, J. Reichert, and K. P. Hofmann. 1982. Complex formation between metarhodopsin II and GTP-binding protein in bovine photoreceptor membranes leads to a shift of the photoproduct equilibirum. *FEBS* (*Fed. Eur. Biochem. Soc.*) *Lett.* 143:29–34.
26. Chabre, M., M. Vuong, and L. Stryer. 1982. Anisotropy of the infrared light-scattering changes induced by illumination of oriented retinal rod outer segments (ROS). *Biophys. J.* 37(2, Pt. 2):274*a*. (Abstr.)